8-17-2018

Three-Dimensional Hybrid Simulation of Viscous-Like Processes at Saturn's Magnetosphere Boundary

P. A. Delamere
University of Alaska, Fairbanks

B. Burkholder
University of Alaska, Fairbanks

X. Ma
Embry-Riddle Aeronautical University, max@erau.edu

Scholarly Commons Citation

Delamere, P. A., Burkholder, B., & Ma, X. (2018). Three-dimensional hybrid simulation of viscous-like processes at Saturn's magnetopause boundary. Geophysical Research Letters, 45, 7901–7908. https://doi.org/10.1029/2018GL078922

Geophysical Research Letters

RESEARCH LETTER
10.1029/2018GL078922

Three-Dimensional Hybrid Simulation of Viscous-Like Processes at Saturn's Magnetopause Boundary

P. A. Delamere[1], B. Burkholder[1], and X. Ma[2]

[1]Geophysical Institute, University of Alaska Fairbanks, Fairbanks, AK, USA, [2]Department of Physical Sciences, Embry-Riddle Aeronautical University, Daytona Beach, FL, USA

Key Points:
- Saturn's magnetosheath flow exhibits a significant dawn/dusk flow asymmetry due to viscous-like stresses
- Momentum transfer rates from hybrid simulations of Saturn's magnetopause boundary yield a significant magnetosheath flow reduction
- Small-scale and intermittent reconnection is at the root of a viscous-like interaction, generating Maxwell shear stresses

Correspondence to:
P. A. Delamere,
padelamere@alaska.edu

Citation:
Delamere, P. A., Burkholder, B., & Ma, X. (2018). Three-dimensional hybrid simulation of viscous-like processes at Saturn's magnetopause boundary. *Geophysical Research Letters*, *45*, 7901–7908. https://doi.org/10.1029/2018GL078922

Received 4 JUN 2018
Accepted 9 JUL 2018
Accepted article online 16 JUL 2018
Published online 17 AUG 2018

Abstract Saturn's magnetosheath flows exhibit significant dawn/dusk asymmetry. The dawnside flows are reduced from expectation, suggesting significant momentum transport through the magnetopause boundary where the flow shear is maximized. It has been suggested that the solar wind interaction with the giant magnetospheres is, in fact, dominated by a viscous-like interaction governed by the Kelvin-Helmholtz instability. In three dimensions, the Kelvin-Helmholtz instability can generate small-scale and intermittent magnetic reconnection due, in part, to a twisted magnetic field topology. The net result is a field line threading of the magnetopause boundary and the generation of Maxwell shear stresses. Here we present three-dimensional hybrid simulations (kinetic ions and massless fluid electrons) of conditions similar to Saturn's dawnside magnetopause boundary to quantify the viscous-like, tangential drag. Using model-determined momentum fluxes, we estimate the effect on dawnside sheath flows and find very good agreement with observations.

Plain Language Summary Planets with magnetic fields generate a cavity in space known as a magnetosphere. At Earth, the solar wind is capable of flowing around the magnetospheric obstacle with minimal drag along the equatorial flanks. This does not appear to be the case at Saturn. A significant solar wind flow asymmetry was observed with the Cassini Spacecraft, indicating substantial drag on the dawnside boundary. Using high-resolution computer simulations that capture individual charged particle (ion) motion, we have demonstrated the basic physical processes responsible for this drag force. We find that strong flow shears generate vortices (i.e., the Kelvin-Helmholtz instability) that twist the magnetic field, directly connecting the solar wind and planetary magnetic fields in an intermittent and patchy manner. The drag force on the solar wind flow is estimated and found to be in good agreement with the simulations. This is the first three-dimensional computer simulation of Saturn's interaction with the solar wind that includes individual charged particle motion. Previous simulations have been limited to two dimensions and did not capture the complicated magnetic connectivity between Saturn and the solar wind.

1. Introduction

The solar wind interaction with Saturn's magnetosphere involves substantial tangential drag at the dawnside magnetopause boundary (Burkholder et al., 2017). In collisionless plasmas, the tangential drag can be described as viscous-like (Axford & Hines, 1961); however, the specific physical mechanisms that allow momentum transport at the magnetopause boundary are poorly understood. The strong flow shears on the dawnside magnetopause boundary suggest that the Kelvin-Helmholtz (KH) instability may play a key role (Delamere et al., 2011; Ma et al., 2015; Masters et al., 2010, 2012, 2014; Wilson et al., 2012). Recent studies to quantify sheared flow-driven transport have demonstrated that in three dimensions the interaction between the KH instability and magnetic reconnection can lead to significant mass transport facilitated through intermittent, midlatitude reconnection (Ma et al., 2017). Typically, the equatorial regions are KH unstable, while midlatitude and high-latitude regions are KH stable (Desroche et al., 2013). This means that interplanetary magnetic field and magnetospheric magnetic fields are twisted locally, forming a pair of strong guide field (component) reconnection sites at midlatitudes. Reconnection can occur asynchronously, generating open flux; however, Ma et al. (2017) showed in three-dimensional (3-D) magnetohydrodynamic (MHD) simulations that double (synchronous) reconnection dominated. The synchronous reconnection allows for plasma transport through flux tube exchange between the reconnection sites.

Ma et al. (2017) found diffusion coefficients under northward interplanetary magnetic field conditions at Earth to be as high as 10^{10} m^2/s.

Recently, global MHD simulations have demonstrated a viscous-like interaction at Saturn's dawnside magnetopause boundary. Using the Block Adaptive Tree Solar wind Roe-type Upwind Scheme (BATS-R-US) 3-D MHD model, Sulaiman et al. (2017) demonstrated a dawn-dusk asymmetry in Saturn's sheath flows immediately adjacent to the magnetopause boundary with terminator flank values approaching 50% of the solar wind speed but with the dawnside ($\sim$ 10 local time) experiencing roughly a factor of 2 reduction in flow speed compared to the dusk ($\sim$ 14 local time). Similarly, using the multifluid Lyon-Fedder-Mobarry (MFLFM) 3-D MHD model for Jupiter, Zhang et al. (2018) showed an even larger (3 times) asymmetry at the same 10 and 14 local time locations. Using sheath flows derived from the Cassini Plasma Spectrometer instrument, Burkholder et al. (2017) showed that, on average, the dawn sector is reduced by a factor of < 2 compared with the dusk sector immediately adjacent to the magnetopause boundary; however, there are instances where the asymmetry exceeds 3 times, indicating substantial variability. The average reduction in dawnside flow (compared with dusk) for all data points taken within 500 min of the magnetopause boundary crossing was 55 km/s. Assuming a spacecraft velocity of 6 km/s and a static magnetopause boundary location, this corresponds to a region of roughly 3 R_S (Saturn radii). A corresponding region inside of the bow shock shows dawn-dusk symmetry.

While the global simulations appear to capture the dawn-dusk asymmetry, there remains the issue of the specific physical mechanism responsible for the momentum transport. On relatively coarse simulation grids, the global simulations are subject to numerical diffusion, yielding an effective viscosity. While the numerics may capture the qualitative nature of the interaction, an elucidation of the specific physical mechanisms is lacking. It is the intent of this paper to demonstrate the momentum transport mechanism using high-resolution 3-D hybrid simulations of Saturn's dawnside magnetopause boundary. Specifically, we initialize a local simulation with parameters representative of Saturn's dawnside magnetopause and directly calculate the momentum transport under a variety of conditions. We find that momentum transport is dominated by off-diagonal (shear stresses) terms in the Maxwell and Reynolds stress tensors. These terms are often comparable, and we will show that the momentum transport is consistent with observations.

The results of this study have broad application to dawn/dusk asymmetries in Jupiter's magnetosphere and the ongoing Juno mission. Comparative studies are also directly relevant to the viscous-like processes at Earth's magnetopause boundary.

1.1. Hybrid Simulation

The hybrid code (kinetic ions and massless fluid electrons) was first proposed by Harned (1982), and the particular algorithms for our code were developed by Swift, (1995, 1996), Delamere (2009), and Delamere et al. (1999). The code assumes quasi-neutrality and is nonradiative. The Lorentz force equation is solved following the Boris method (Birdsall & Langdon, 1991; Boris, 1970). The electric field and magnetic fields are calculated on a Yee grid (Yee, 1966), ensuring easy curl calculations while maintaining a divergence-free magnetic field. The magnetic field equations are updated with a second-order, predictor-corrector method. Specifically, the particles are advanced by the ion equation of motion $m_i \frac{d\mathbf{v}_i}{dt} = q(\mathbf{E}+\mathbf{v}_i \times \mathbf{B})$ where $\mathbf{v}_i$ is the ion particle velocity, $\mathbf{E}$ is the electric field, $\mathbf{B}$ is the magnetic field, m_i is the ion mass, and q is the elementary charge. The massless electron momentum equation is used to find the electric field, $\mathbf{E} = -\mathbf{u}_e \times \mathbf{B} - \nu(\mathbf{u}_e - \mathbf{u}_i) - \nabla P_e/(nq)$ where $\mathbf{u}_e$ and P_e are the electron flow velocity and thermal pressure and ν is the electron-ion collision frequency. The electron fluid is assumed to be isothermal such that $\nabla P_e = T_e \nabla n$. Ampere's law is $\mathbf{u}_e = \mathbf{u}_i - \frac{1}{\mu_o nq} \nabla \times \mathbf{B}$ where $\mathbf{u}_i$ is the ion bulk flow velocity determined with standard particle-in-cell shape functions (i.e., particle to grid weighting). The magnetic field is advanced from Faraday's law.

We note that electron pressure effects can be captured by the hybrid simulation to model kinetic Alfvén waves (KAWs). For instance, in the high electron beta approximation, the dispersion relation for the KAW is $\omega^2 \approx k_\parallel^2 v_A^2 \left[1 + \left(1 + T_e/T_i\right) k_\perp^2 \rho_i^2\right]$ where ρ_i is the ion Larmor radius and v_A is the Alfvén speed. In addition, at ion inertial scales the kinetic Alfvén mode resolves the Alfvén and ion-ion hybrid resonances of the fast magnetosonic/whistler branch. The hybrid code captures kinetic aspects of magnetopause boundary processes including mode conversion of compressional fast mode waves to KAWs.

The 3-D simulations used in this study follow from the two-dimensional simulations of KH by Delamere et al. (2011) where the magnetic field was primarily in the ignorable (y) direction. Here we expand the simulation domain along the magnetic field y direction and include a small magnetic field component in the flow

Table 1
Simulation Parameters

Parameters	Values
Mass, (AMU)	1
Density, n_p (10^6 m^{-3})	0.4
Mass density, ρ_o (10^{-22} kg/m^3)	6.7
Ion inertial length, c/ω_{pi} (km)	360
Magnetic field, B_0 (nT)	5
Alfvén speed, v_A (km/s)	173
Plasma β	1
Initial in-plane magnetic field, B_{x0} (nT)	0.2
Magnetic shear profile	$B_{x0}\tanh[(z-z_0)/L_0]$
Velocity shear layer profile	$0.8v_A\tanh[(z-z_0)/L_0]$
Scale length of shear profile, L_o	$1.0c/\omega_{pi}$
Grid resolution	$0.5c/\omega_{pi}$
Electron temperature (eV)	10

shear plane (*xz*). The *x* and *y* boundary conditions are periodic. The *z* boundary is open with $\partial_z = 0$. The flow shear profile is given by $0.8v_A\tanh[(z-z_0)/L_0]$, where v_A is the magnetosheath Alfvén velocity and L_0 is the scale of the velocity jump. The magnetic field is nearly parallel with a small sheared in-plane B_x component. Table 1 summarizes our baseline parameters that are representative of Saturn's dawnside magnetopause boundary. In this paper we only consider the thermal plasma (protons only) as a baseline case. A more realistic simulation for future study would include heavy ions (Delamere et al., 2011) and the superthermal population (Sergis et al., 2013). We anticipate that heavy and/or superthermal ions will increase diffusive transport, potentially enhancing the viscous-like interaction. We use a plasma $\beta \sim 1$ following observations of the thermal plasma (Wilson et al., 2012) and a grid resolution of $0.5c/\omega_{pi}$, where c/ω_{pi} is the ion inertial length. Under these conditions the proton thermal gyromotion is resolved.

2. Results

Figure 1 shows an example from a 3-D simulation at $t = 88(\Omega_i^{-1})$. The color slices in the *xz* plane show particle mixing. Particles are initialized with values of 0 (blue) or 1 (red) depending on location with respect to the velocity shear boundary, and thus intermediate colors indicate the extent of mixing. The KH vortices quickly mix the plasma (e.g., *superdiffusion* described by Cowee et al., 2010) due to large ion gyroradius effects and relatively thin boundaries. The gray isosurface indicates the 50% mixing boundary and serves as a proxy for the distorted magnetopause boundary. Magnetic field lines (colored by local mixing) are shown, traced from the bottom to top boundary. The variation in the *y* direction is evident as is the twisting of the magnetic field. The patchy red isosurfaces indicate regions with parallel electric fields and thus regions where strong guide field/component reconnection is occurring.

Hybrid simulations of the KH instability are self seeding. That is, the surface waves grow from the random fluctuations associated with coarse particle statistics and typically appear initially at the shortest wavelength resolved by the grid ($\sim 1.5c/\omega_{pi}$). The fastest growing mode in a compressible plasma ranges between k_xL_0 and $2k_xL_0$ or 6 to 12 c/ω_{pi} (Miura & Pritchett, 1982). Larger wavelengths have lower growth rates but larger amplitudes, resulting in an inverse cascade to larger scales (Delamere et al., 2011). Figure 2 shows a power spectrum of perpendicular (i.e., B_x, B_z) magnetic field fluctuations at $t = 192\Omega_i^{-1}$. The dotted vertical line corresponds to $k_x = \pi/(c/\omega_{pi})$. The red line has a spectral index of −5/3, and the blue line has a spectral index of −8/3 consistent with a turbulent cascade in the respective inertial and dissipative ranges (Galtier et al., 2005). Turbulent magnetic fluctuations are seen throughout Saturn's magnetosphere (Kaminker et al., 2017; von Papen et al., 2014), and KH-related ion heating could be an important aspect of boundary layer processes.

The phase of the surface waves also varies along the magnetic field due to the stochastic nature of the initial perturbation. Figure 3 shows the *xy* plane taken from the center of flow shear region at $t = 64\Omega_i^{-1}$, illustrating

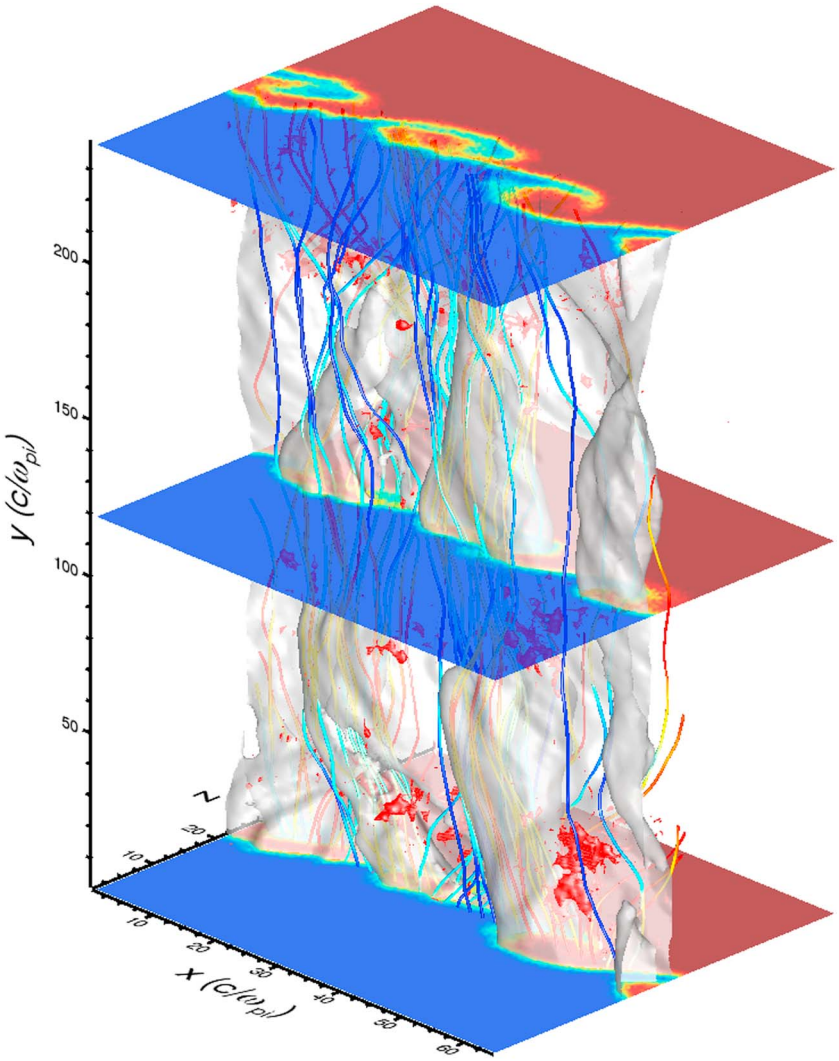

Figure 1. Results from the 3-D hybrid Kelvin-Helmholtz simulation at $t = 88(\Omega_i^{-1})$. The color slices indicate particle mixing, the gray surface is the 50% mixing boundary (i.e., magnetopause), the red isosurfaces are regions of parallel electric fields, and the sample magnetic field lines are colored by particle mixing.

the field-aligned structure of B_x, u_x, and the particle mixing. A surface wave that is 180° out of phase with a wave in another region will locally twist the magnetic field, potentially leading to strong guide field reconnection. The reconnection process is similar to the double reconnection process discussed by Ma et al. (2017) for the KH instability at Earth. However, in this case reconnection can occur in many locations if $k_{\|}$ is large. Due to the limited box size, the simulations eventually saturate at an $m = 1$ mode and the parallel dimension can also be considered ignorable. In reality, the KH waves can continue to grow and $k_{\|}$ is determined, in part, by the extent of the KH unstable region of the magnetopause boundary (Desroche et al., 2013).

An estimate of the momentum transfer can be made by considering the flux conservative form of the momentum equation in steady state

$$\cancelto{0}{\frac{\partial \rho \mathbf{u}}{\partial t}} + \nabla \cdot \left[\rho \mathbf{u}\mathbf{u} + \mathbf{P} + \frac{B^2}{2\mu_o}\mathbf{I} - \frac{\mathbf{B}\mathbf{B}}{\mu_o} \right] = 0. \tag{1}$$

Strictly speaking, the KH instability is a dynamic process, but we treat the average state of the magnetopause boundary as static (i.e., between the limits of a diffuse boundary layer and actively growing vortices).

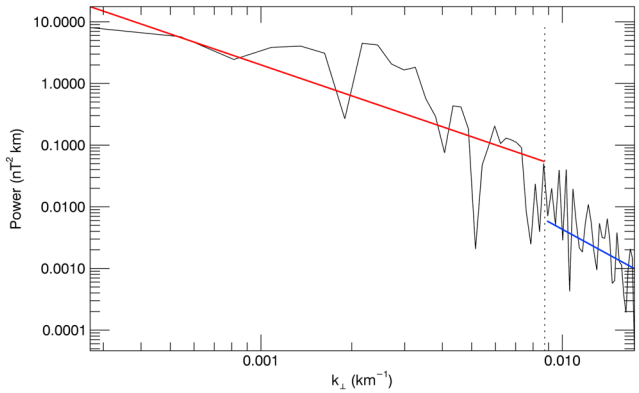

Figure 2. Power spectrum of magnetic field fluctuations in the central vortex region at $t = 152(\Omega_i^{-1})$. The dotted vertical line corresponds to $k_\perp = \pi/(c/\omega_{pi})$. The red line has a spectral index of −5/3, and the blue line has a spectral index of −8/3.

The volume integral of the steady state momentum equation can be written as a surface integral via the divergence theorem,

$$\int \nabla \cdot \left[\rho \mathbf{uu} + \mathbf{P} + \frac{B^2}{2\mu_o}\mathbf{I} - \frac{\mathbf{BB}}{\mu_o}\right] dV = \oint \left[\rho \mathbf{uu} + \mathbf{P} + \frac{B^2}{2\mu_o}\mathbf{I} - \frac{\mathbf{BB}}{\mu_o}\right] \cdot d\mathbf{a} = 0. \quad (2)$$

Here we integrate over the central *xz* plane shown in Figure 3, comparing the off-diagonal elements of the $\rho\mathbf{uu}$ (Reynolds) and $\mathbf{BB}/\mu_o$ (Maxwell) terms. Specifically, we are interested in tangential *x*-directed momentum transported in the normal *z* direction, or $T^R_{xz} = \rho u_x u_z$ and $T^M_{xz} = B_x B_z/\mu_o$. Figure 4 compares T^M_{xz} with T^R_{xz} as a function of time, showing the overall net positive contribution of the Maxwell stresses, though the

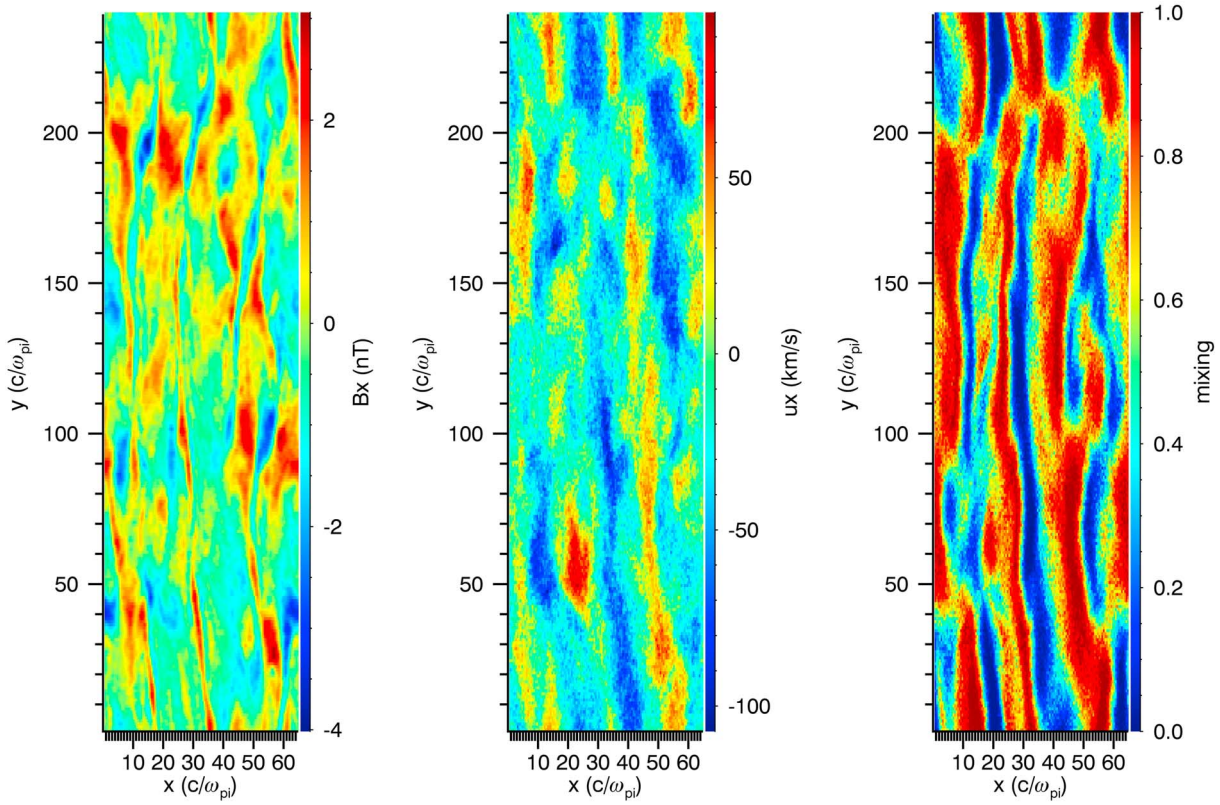

Figure 3. The central *xy* plane taken at $t = 64(\Omega_i^{-1})$, showing B_x, u_x, and mixing. The phase of the Kelvin-Helmholtz waves varies in the *y* direction generating significant structure in the field-aligned direction.

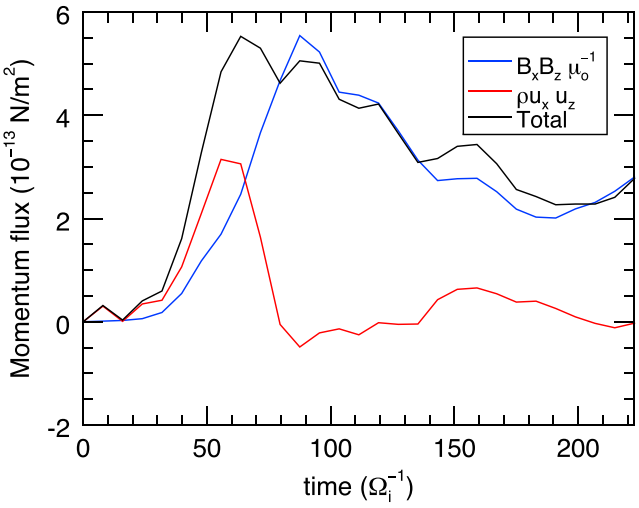

Figure 4. Shear stresses as a function of time. Both Reynolds (T^R_{xz}) and Maxwell (T^M_{xz}) stresses contribute to the momentum transport, but T^M_{xz} provides the dominant contribution.

Reynolds stresses also contribute. The momentum fluxes increase rapidly as the instability progresses through the inverse cascade but at later times decrease as the simulation saturates in the $m = 1$ mode.

3. Estimate of Dawnside Sheath Flow Reduction

An estimate of the effect on Saturn's dawnside sheath flow can be made using the momentum transport rate from the hybrid simulations. Following Figure 5, we let $+\hat{\mathbf{t}}$ (tangential) be toward the subsolar point and $+\hat{\mathbf{n}}$ (normal) be toward the planet (simulation coordinates). Assume a volume of the sheath with equal inflow (subscript 1) and outflow (subscript 2) areas with width L_t and area $a_t = L_t\delta z$ where δz is the vertical scale of the KH unstable region of the magnetopause boundary. The area on the magnetopause boundary (subscript 3) is $a_n = L_n dz$, so the ratio of the areas is, for example, L_n/L_t.

For the case of no viscous stress (on the magnetopause boundary surface a_n) the tangential component of the force balance equation (equation (2)) is

$$\rho_1 u_1^2 a_t - \rho_2 u_2^2 a_t + P_1 a_t - P_2 a_t = 0. \tag{3}$$

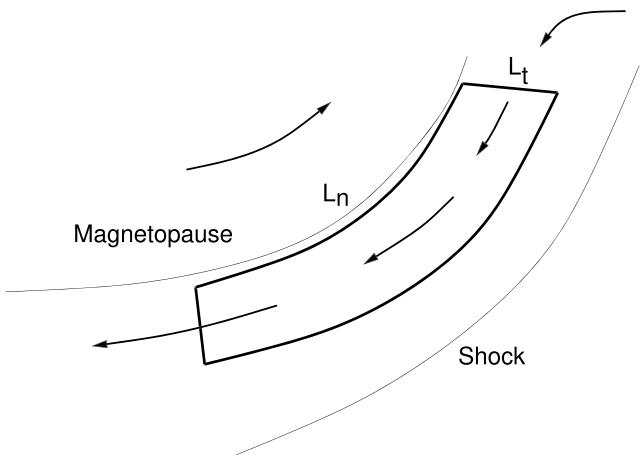

Figure 5. An equatorial cross section of the volume considered for evaluating the momentum transport to Saturn's dawnside magnetosheath.

If we assume that $\rho_1 u_1^2 \ll \rho_2 u_2^2$ (assume negligible dynamic pressure at inflow boundary, okay for subsolar point), then the pressure difference can be expressed in terms of the asymptotic sheath flow, u_2, or

$$\rho_2 u_2^2 = P_1 - P_2, \tag{4}$$

where P represents both thermal plasma pressure and magnetic pressure associated with MHD flow of shocked plasma in the sheath.

Now consider the case where viscous stresses (tangential drag) are present on the magnetopause boundary, but assume that P_1 and P_2 are unchanged due to modified flow. For the sake of a rough estimate (upper limit), we assume that equation (4) is valid and equation (2) becomes

$$P_1 a_t - P_2 a_t - \rho_2 (u_2')^2 a_t - \frac{B_n B_t}{\mu_o} a_n + \rho_3 u_n u_t a_n = 0, \tag{5}$$

which implies

$$(\Delta u_2)^2 = \frac{1}{\rho_2}\left(\frac{B_n B_t}{\mu_o} - \rho_3 u_n u_t\right)\frac{a_n}{a_t}, \tag{6}$$

where $(\Delta u_2)^2 = u_2^2 - (u_2')^2$ and where ρ_3 is the mass density on the magnetopause boundary.

Typical upper limit values for the Maxwell and Reynolds stresses on the right-hand side from the hybrid simulations are 4×10^{-13} N/m^2, the average sheath mass density is $\rho_2 = 0.18$ cm^{-3}, and $a_n/a_t = L_n/L_t \sim 15/3 = 5$. For these parameters $\Delta u_2 \sim 80$ km/s. This is consistent with the observed flow reduction in Saturn's dawnside magnetosheath where the expected asymptotic flow is 200 km/s.

4. Conclusions

The viscous-like interaction between the solar wind and Saturn's magnetosphere is manifested by significant dawn-dusk asymmetries in magnetosheath flows (Burkholder et al., 2017). Using a 3-D hybrid simulation, we have quantified the momentum transport at Saturn's KH unstable magnetopause boundary. We conclude as follows:

1. At the root of the viscous-like interaction are Maxwell shear stresses generated at the magnetopause boundary by magnetic field line threading.
2. Small-scale and intermittent reconnection facilitate field line threading of the boundary at multiple reconnection sites.
3. Magnetic field fluctuations are turbulent, and plasma heating is expected.
4. Diffusive plasma transport leads to a rapid mixing of magnetosphere and solar wind plasma.
5. The episodic nature of the KH instability may account for the wide range of dawnside sheath flows reported by Burkholder et al. (2017).

Future studies will investigate the effect of heavy and/or superthermal ions as well as turbulent heating and associated diffusive transport. Momentum fluxes from our local simulations will also be compared with global simulations (e.g., Zhang et al., 2018) to determine whether numerical effects (i.e., viscosity) are an accurate approximation to the realistic kinetic-scale physics that cannot be resolved in global simulations.

Acknowledgments
The authors acknowledge support from NASA grants NNX15AH09G and NNX17AI50G and are grateful to the International Space Science Institute (ISSI) for their support to the Coordinated Numerical Modeling of the Global Jovian and Saturnian Systems team. The model source code in this paper can be accessed from the corresponding author at padelamere@alaska.edu or at https://github.com/padelamere.

References

Axford, W. I., & Hines, C. O. (1961). A unifying theory of high latitude geophysical phenomena and geomagnetic storms. *Canadian Journal of Physics*, *39*, 1433–1464.

Birdsall, C. K., & Langdon, A. B. (1991). *Plasma physics via computer simulation*. Boca Raton: CRC Press.

Boris, J. P. (1970). Relativistic plasma simulation-optimization of a hybrid code. In *Proceedings of the 4th Conference on Numerical Simulation of Plasmas* (pp. 3–67.). Washington, DC: Naval Research Laboratory.

Burkholder, B., Delamere, P. A., Ma, X., Thomsen, M. F., Wilson, R. J., & Bagenal, F. (2017). Local time asymmetry of Saturn's magnetosheath flows. *Geophysical Research Letters*, *44*, 5877–5883. https://doi.org/10.1002/2017GL073031

Cowee, M. M., Winske, D., & Gary, S. P. (2010). Hybrid simulations of plasma transport by Kelvin-Helmholtz instability at the magnetopause: Density variations and magnetic shear. *Journal of Geophysical Research*, *115*, 6214. https://doi.org/10.1029/2009JA015011

Delamere, P. A. (2009). Hybrid code simulations of the solar wind interaction with Pluto. *Journal of Geophysical Research: Space Physics*, *114*, A03220. https://doi.org/10.1029/2008JA013756

Delamere, P. A., Swift, D. W., & Stenbaek-Nielsen, H. C. (1999). A three-dimensional hybrid code simulation of the December 1984 solar wind AMPTE release. *Geophysical Research Letter*, *26*, 2837–2840. https://doi,org/10.1029/1999GL900602

Delamere, P. A., Wilson, R. J., & Masters, A. (2011). Kelvin-Helmholtz instability at Saturn's magnetopause: Hybrid simulations. *Journal of Geophysical Research*, *116*, A10222. https://doi.org/10.1029/2011JA016724

Desroche, M., Bagenal, F., Delamere, P. A., & Erkaev, N. (2013). Conditions at the magnetopause of Saturn and implications for the solar wind interaction. *Journal of Geophysical Research: Space Physics*, *118*, 3087–3095. https://doi.org/10.1002/jgra.50294

Galtier, S., Pouquet, A., & Mangeney, A. (2005). On spectral scaling laws for incompressible anisotropic magnetohydrodynamic turbulence. *Physics of Plasmas*, *12*, 092310.

Harned, D. S. (1982). Quasineutral hybrid simulation of macroscopic plasma phenomena. *Journal of Computational Physics*, *47*, 452.

Kaminker, V., Delamere, P. A., Ng, C. S., Dennis, T., Otto, A., & Ma, X. (2017). Local time dependence of turbulent magnetic fields in Saturn's magnetodisc. *Journal of Geophysical Research: Space Physics*, *122*, 3972–3984. https://doi.org/10.1002/2016JA023834

Ma, X., Delamere, P., Otto, A., & Burkholder, B. (2017). Plasma transport driven by the three-dimensional Kelvin-Helmholtz instability. *Journal of Geophysical Research: Space Physics*, *122*, 10. https://doi.org/10.1002/2017JA024394

Ma, X., Stauffer, B., Delamere, P. A., & Otto, A. (2015). Asymmetric Kelvin-Helmholtz propagation at Saturn's dayside magnetopause. *Journal of Geophysical Research: Space Physics*, *120*, 1867–1875. https://doi.org/10.1002/2014JA020746

Masters, A., Achilleos, N., Cutler, J. C., Coates, A. J., Dougherty, M. K., & Jones, G. H. (2012). Surface waves on Saturn's magnetopause. *Planetary and Space Science*, *65*, 109–121. https://doi.org/10.1016/j.pss.2012.02.007

Masters, A., Achilleos, N., Kivelson, M. G., Sergis, N., Dougherty, M. K., Thomsen, M. F., et al. (2010). Cassini observations of a Kelvin-Helmholtz vortex in Saturn's outer magnetosphere. *Journal of Geophysical Research*, *115*, A07225. https://doi.org/10.1029/2010JA015351

Masters, A., Fujimoto, M., Hasegawa, H., Russell, C. T., Coates, A. J., & Dougherty, M. K. (2014). Can magnetopause reconnection drive Saturn's magnetosphere?. *Geophysical Research Letter*, *41*, 1862–1868. https://doi.org/10.1002/2014GL059288

Miura, A., & Pritchett, P. L. (1982). Nonlocal stability analysis of the MHD Kelvin-Helmholtz instability in a compressible plasma. *Journal of Geophysical Research*, *87*, 7431–7444. https://doi.org/10.1029/JA087iA09p07431

Sergis, N., Jackman, C. M., Masters, A., Krimigis, S. M., Thomsen, M. F., Hamilton, D. C., et al. (2013). Particle and magnetic field properties of the Saturnian magnetosheath: Presence and upstream escape of hot magnetospheric plasma. *Journal of Geophysical Research: Space Physics*, *118*, 1620–1634. https://doi.org/10.1002/jgra.50164

Sulaiman, A. H., Jia, X., Achilleos, N., Sergis, N., Gurnett, D. A., & Kurth, W. S. (2017). Large-scale solar wind flow around Saturn's nonaxisymmetric magnetosphere. *Journal of Geophysical Research: Space Physics*, *122*, 9198–9206. https://doi.org/10.1002/2017JA024595

Swift, D. W. (1995). Use of a hybrid code to model the Earth's magnetosphere. *Geophysical Research Letter*, *22*, 311.

Swift, D. W. (1996). Use of a hybrid code for global-scale plasma simulation. *Journal of Computational Physics*, *126*, 109.

von Papen, M., Saur, J., & Alexandrova, O. (2014). Turbulent magnetic field fluctuations in Saturn's magnetosphere. *Journal of Geophysical Research: Space Physics*, *119*, 2797–2818. https://doi.org/10.1002/2013JA019542

Wilson, R. J., Delamere, P. A., Bagenal, F., & Masters, A. (2012). Kelvin-Helmholtz instability at Saturn's magnetopause: Cassini ion data analysis. *Journal of Geophysical Research*, *117*, A03212. https://doi.org/10.1029/2011JA016723

Yee, K. (1966). Numerical solution of initial boundary value problems involving Maxwell's equations in isotropic media. *IEEE Transactions on Antennas and Propagation*, *14*, 302–307. https://doi.org/10.1109/TAP.1966.1138693

Zhang, B., Delamere, P. A., Ma, X., Burkholder, B., Wiltberger, M., Lyon, J. G., et al. (2018). Asymmetric Kelvin-Helmholtz instability at Jupiter's magnetopause boundary: Implications for corotation-dominated systems. *Geophysical Research Letters*, *45*, 56–63. https://doi.org/10.1002/2017GL076315